BEILSTEIN ARCHIVES

This open access document is posted as a preprint in the Beilstein Archives at https://doi.org/10.3762/bxiv.2026.5.v1 and is considered to be an early communication for feedback before peer review. Before citing this document, please check if a final, peer-reviewed version has been published.

This document is not formatted, has not undergone copyediting or typesetting, and may contain errors, unsubstantiated scientific claims or preliminary data.

Preprint Title Oxidative Atmosphere-Driven Formation of Single-Phase Spinel $CuRh_2O_4$ Nanofibers for Alkaline Water Oxidation

Authors Namhee Kim, Myung Hwa Kim and Dasol Jin

Publication Date 28 Jan. 2026

Article Type Full Research Paper

ORCID® iDs Namhee Kim - https://orcid.org/0009-0000-1969-4370; Myung Hwa Kim - https://orcid.org/0000-0001-7254-2886

License and Terms: This document is copyright 2026 the Author(s); licensee Beilstein-Institut.

This is an open access work under the terms of the Creative Commons Attribution License (https://creativecommons.org/licenses/by/4.0). Please note that the reuse, redistribution and reproduction in particular requires that the author(s) and source are credited and that individual graphics may be subject to special legal provisions. The license is subject to the Beilstein Archives terms and conditions: https://www.beilstein-archives.org/xiv/terms.
The definitive version of this work can be found at https://doi.org/10.3762/bxiv.2026.5.v1

Oxidative Atmosphere-Driven Formation of Single-Phase Spinel $CuRh_2O_4$ Nanofibers for Alkaline Water Oxidation

Namhee Kim[1], Myung Hwa Kim[1,2,*] and Dasol Jin[3,*]

Address: [1]Department of Chemistry and Nanoscience, Ewha Womans University, Seoul 03760, Republic of Korea

[2]Institute of Multiscale Matter and System (IMMS), Ewha Womans University, Seoul 03760, Republic of Korea

[3]Department of Chemistry, Jeonbuk National University, Jeonju 54896, Republic of Korea

Email: Dasol Jin (dasoljin@jbnu.ac.kr) and Myung Hwa Kim (myungkim@ewha.ac.kr)

* Corresponding author

Abstract

Cu–Rh bimetallic single-phase spinel oxide nanofibers were synthesized *via* electrospinning followed by post-annealing under precisely controlled oxidative environments. By systematically tuning the O_2 concentration in He carrier flow during the annealing process, the optimal atmosphere was identified to produce phase-pure $CuRh_2O_4$. The as-prepared $CuRh_2O_4$ nanofibers exhibited excellent electrocatalytic performance toward the oxygen evolution reaction in 1.0 M NaOH (*aq*), highlighting

the importance of atmosphere-controlled thermal treatment for engineering high-activity spinel oxide electrocatalysts.

Keywords

annealing; electrospinning; spinel oxide; oxygen evolution reaction; electrocatalyst

Introduction

Oxygen evolution reaction (OER) is a kinetically demanding, multistep process that governs the efficiency of alkaline water electrolysis [1]. Developing robust and highly active OER electrocatalysts is therefore essential for practical hydrogen production and large-scale renewable energy conversion. Among numerous catalyst platforms, spinel oxides (AB_2O_4) have attracted significant attention due to their structural robustness and compositional tunability [2]. The spinel framework accommodates diverse metal cations with flexible site occupancy, enabling rational modulation of electronic structure and surface adsorption energetics of key OER intermediates [3], thereby offering a versatile strategy for performance optimization.

Despite these advantages, synthesizing phase-pure spinel oxides remains challenging when Cu is incorporated. Cu-based catalysts are particularly sensitive to the synthetic environment because Cu readily changes its oxidation state ($Cu^0/Cu^+/Cu^{2+}$) depending on the oxidative atmosphere during annealing [4,5]. As a result, slight variations in oxygen partial pressure can significantly alter phase evolution and often lead to undesired secondary phases (*e.g.*, CuO or Cu_2O) [6]. Thus, establishing an atmosphere-controlled synthesis route is critical for producing single-phase Cu-containing spinel oxides with reliable and optimized electrocatalytic properties.

Herein, we demonstrate the synthesis of Cu–Rh bimetallic single-phase spinel oxide nanofibers *via* electrospinning followed by post-annealing under precisely controlled oxidative environments. By deliberately controlling the annealing atmosphere under the continuous O_2/He flow, optimized conditions were identified to obtain single-phase $CuRh_2O_4$ nanofibers. The resulting spinel oxides exhibit excellent OER electrocatalytic activity in 1 M NaOH (*aq*), highlighting the importance of oxygen-atmosphere engineering for the rational design of Cu-based spinel oxide catalysts.

Results and Discussion

A series of Cu–Rh bimetallic oxide nanofibers were synthesized *via* electrospinning and subsequent annealing process under continuous O_2/He flow, as illustrated in Figure 1 (see *Experimental* section for details).

As shown in Figure 2, XRD was employed to investigate the phase evolution of Cu–Rh oxide nanofibers annealed under different oxidative environments (*i.e.*, O_2 concentrations of 5.6%, 11.1% and 22.2%). The diffraction patterns reveal that the O_2 concentration during annealing plays a decisive role in determining the crystallographic phase and phase purity. Under insufficient oxidative condition (*i.e.*, O_2 5.6%), additional

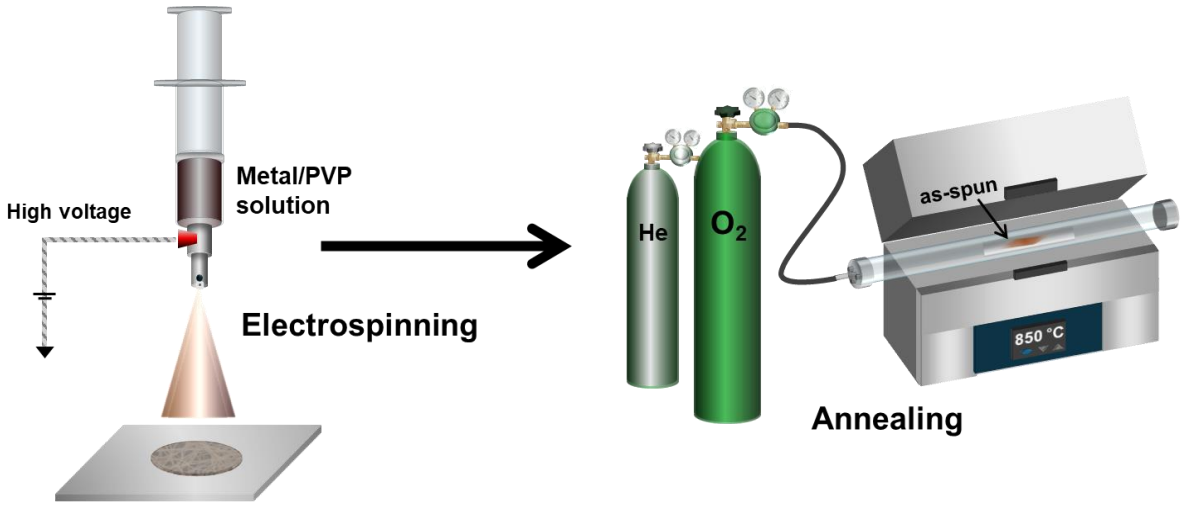

Figure 1. Schematic illustration of the synthesis procedure used in this study.

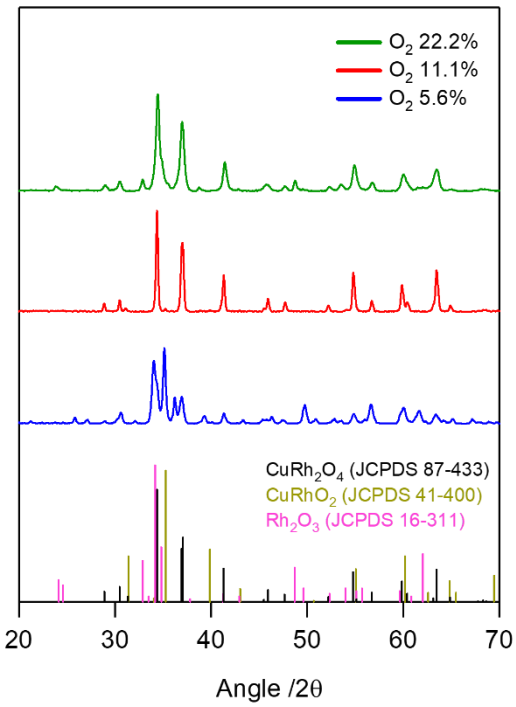

Figure 2. XRD patterns of as-prepared nanomaterials synthesized under different O_2 concentrations. Unassigned peaks suggest the presence of secondary copper oxide phases (Cu_2O/CuO).

patterns attributable to $CuRhO_2$, Rh_2O_3, Rh and Cu_2O are observed, indicating incomplete formation of the targeted spinel structure. In contrast, the optimized oxygen concentration (*i.e.*, O_2 11.1%) yields diffraction peaks that can be fully indexed to spinel $CuRh_2O_4$, confirming the formation of a single-phase crystalline structure. However,

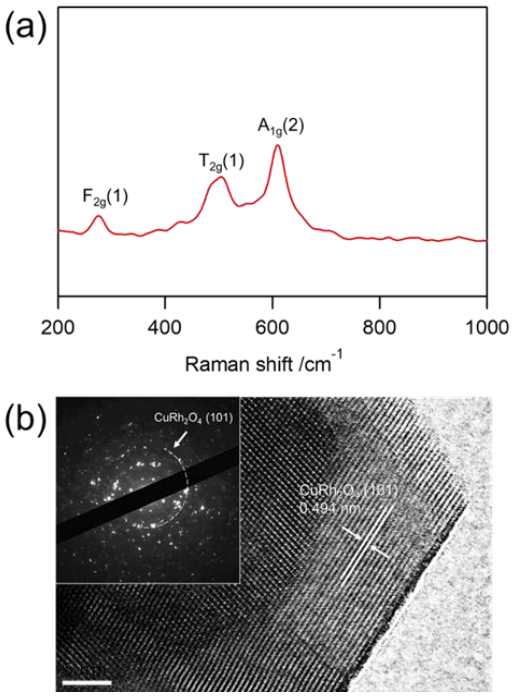

Figure 4. (a) Raman characterization and (b) HRTEM image of nanomaterials annealed under O_2 concentration of 11.1% (inset: corresponding SAED pattern).

under excessive oxidative conditions (*i.e.*, O_2 22.2%), mixed phases consisting of $CuRh_2O_4$ along with $CuRhO_2$ and Rh_2O_3 are observed. These results highlight that precise oxygen-atmosphere engineering during annealing is critical for suppressing undesired phase segregation and achieving phase-pure $CuRh_2O_4$ nanofibers.

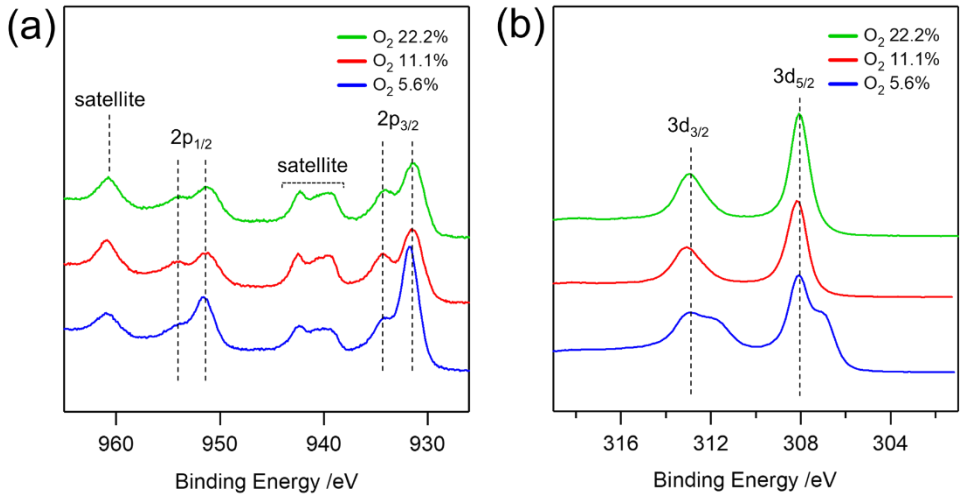

Figure 3. AR-XPS spectra of nanomaterials in (a) Cu 2p and (b) Rh 3d regions.

AR-XPS was performed to clarify the surface chemical states of Cu and Rh in Cu–Rh bimetallic oxides synthesized under different O_2 concentrations. The Cu 2p spectra in Figure 3(a) exhibit distinct Cu $2p_{3/2}$ (*ca.* 935 eV) and Cu $2p_{1/2}$ (*ca.* 952 eV) peaks characteristic of oxidized Cu species, accompanied by shake-up satellite features, indicating predominance of Cu^{2+} on the surface [7,8]. Meanwhile, the Rh 3d spectrum in Figure 3(b) shows well-defined Rh $3d_{5/2}$ (*ca.* 308 eV) and Rh $3d_{3/2}$ (*ca.* 313 eV) doublet peaks, confirming the stable incorporation of Rh^{3+} within the oxide lattice under the optimized annealing condition [9]. In contrast, under the low O_2 concentration (5.6%), additional peaks corresponding to metallic Rh (Rh^0) are observed at around 305 eV, indicating that the oxidative environment is insufficient to fully form the spinel $CuRh_2O_4$ phase [10].

As shown in Figure 4(a), Raman spectroscopy was conducted to further examine the local bonding environments and short-range structural order of the phase-pure $CuRh_2O_4$ nanomaterials synthesized under the optimized condition (*i.e.*, O_2 11.1%). The spectrum exhibits characteristic vibrational modes at 277.6 cm^{-1} (F_{2g}), 501.3 cm^{-1} (T_{2g}) and 609.6 cm^{-1} for (A_{1g}), which are consistent with the spinel $CuRh_2O_4$

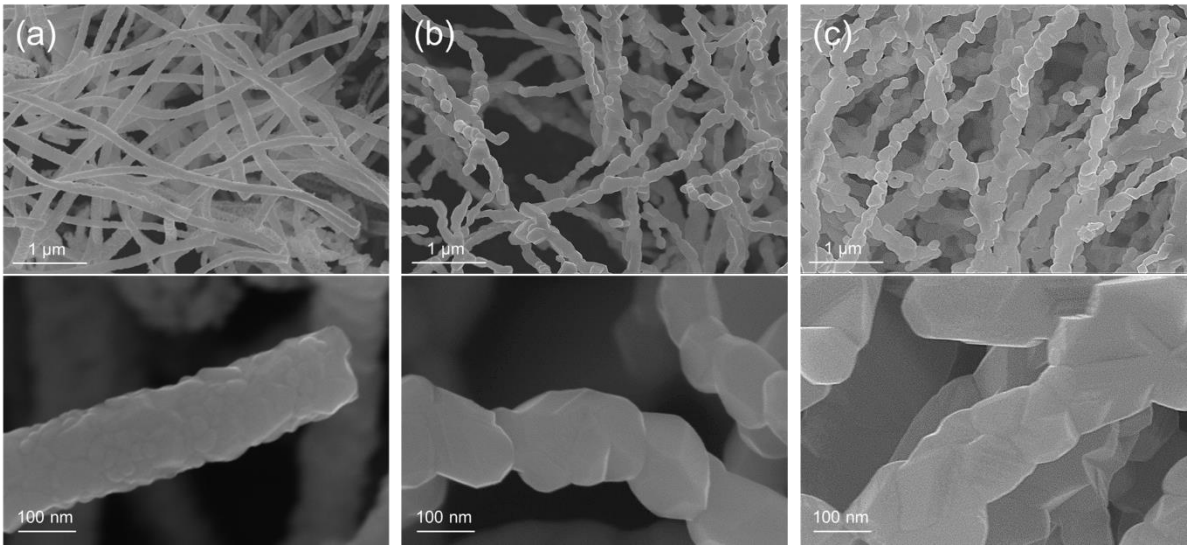

Figure 5. SEM images of the as-prepared nanomaterials synthesized under O_2 concentrations of (a) 5.6%, (b) 11.1%, and (c) 22.2%.

lattice [11,12], supporting the XRD-based phase assignment (*vide supra*). As shown in Figure 4(b), HRTEM analysis of the electrospun $CuRh_2O_4$ nanofibers reveals clear lattice fringes with an interplanar spacing of 0.494 nm, corresponding to (101) plane [13]. Selected area electron diffraction (SAED) patterns display ring-like diffraction features consistent with polycrystalline spinel $CuRh_2O_4$, further verifying the formation of the intended crystalline phase.

As shown in Figure 5, SEM was employed to investigate the surface morphology and structural uniformity of the electrospun nanofibers after post-annealing. The images show continuous and uniform nanofiber structures with well-distributed fiber

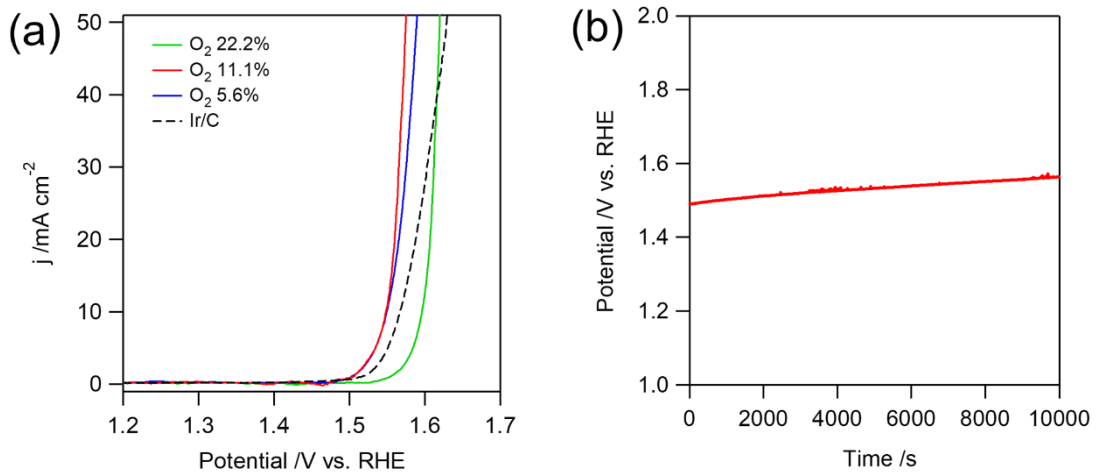

Figure 6. (a) LSV polarization curves of the as-prepared Cu–Rh bimetallic oxides and commercial Ir/C, and (b) chronopotentiometric profile of nanofibers synthesized under 11.1% O_2 in N_2-saturated NaOH (*aq*).

networks. As the O_2 concentration increased (from Figure 5(a) to 5(c)), the surface roughness became more pronounced, suggesting that an oxygen-rich annealing atmosphere significantly affects the topology and growth behavior of the oxide nanocrystals [14]. This observation indicates that the oxidative environment influences not only phase formation but also fiber integrity and surface texture.

The OER electrocatalytic activity of the prepared nanofibers was evaluated in N_2-saturated 1.0 M NaOH (*aq*) using a standard three-electrode configuration. As shown in the *i*R-corrected LSV cures in Figure 6(a), the phase-pure $CuRh_2O_4$ nanofibers prepared under O_2 11.1% exhibit superior OER activity compared to samples containing secondary phases, demonstrating the critical role of phase purity in catalytic performance. Notably, the optimized $CuRh_2O_4$ nanofibers outperform commercial Ir/C, a benchmark catalyst for alkaline OER, requiring lower potential of 1.53 V (vs. RHE) to reach 10 mA cm^{-2}, compared to 1.57 V (vs. RHE) for Ir/C. Additionally, the electrocatalyst demonstrates excellent durability, as shown in Figure 6(b), maintaining a nearly stable potential during 10 000 s of continuous OER operation at a constant current density of 10 mA cm^{-2}.

Conclusion

In summary, Cu–Rh bimetallic single-phase spinel oxide nanofibers were successfully synthesized *via* electrospinning followed by post-annealing under precisely controlled oxidative environments. By deliberately regulating the O_2 concentration in He carrier flow, an optimized annealing condition (*i.e.*, 11.1% O_2) was identified to produce phase-pure $CuRh_2O_4$ nanofibers while preserving the uniform fibrous morphology. Structural and spectroscopic characterizations confirmed the formation of a highly crystalline spinel phase with well-defined nanofiber architecture, and XPS analysis further verified stabilized surface chemical states of Cu and Rh under the optimized annealing atmosphere. Importantly, the phase-pure $CuRh_2O_4$ nanofibers exhibited excellent electrocatalytic activity toward the oxygen evolution reaction in 1 M NaOH. This study highlights oxygen-atmosphere engineering as a critical parameter for the

reproducible synthesis and performance optimization of Cu-based spinel oxide electrocatalysts for alkaline water oxidation.

Experimental

Materials

Copper(II) chloride hexahydrate ($CuCl_2 \cdot 6H_2O$), rhodium(III) chloride hydrate ($RhCl_3 \cdot xH_2O$), poly(vinylpyrrolidone) (PVP, $M_n \approx 1\,300\,000$), sodium hydroxide (NaOH), and Nafion solution (5 wt%) were purchased from Sigma-Aldrich (St. Louis, MO, USA). Ethanol was obtained from Daejung Chemicals (Korea). Commercial Ir/C catalyst (20 wt% metal loading on Vulcan XC-72) was purchased from Premetek Co. (USA). All aqueous solutions were prepared using deionized water (resistivity ≥ 18 MΩ·cm).

Synthesis

Electrospinning solution was prepared by dissolving Rh and Cu metal precursors at molar concentrations (mol/L) of 0.151 and 0.076, respectively, in 2.2 mL of a mixed solvent comprising ethanol (1.5 mL) and deionized water (0.7 mL), followed by ultrasonication for 30 min to achieve complete homogenization. Subsequently, 200 mg of PVP was added to the precursor solution. The mixture was magnetically stirred for 18 h at room temperature to obtain a fully homogenized spinning solution. The prepared precursor solution was then loaded into a plastic syringe and electrospun using an electrospinning system (NanoNC, ESR200R2). Electrospinning was performed at a feed rate of 10 μL min^{-1} with an applied voltage of 17 kV. Finally, the electrospun metal precursor/PVP nanofibers were calcined at 850 °C for 1 h under a continuous mixed gas flow of O_2 and He with controlled O_2 concentrations (5.6%, 11.1% and 22.2%).

Physicochemical Characterization

The morphology and elemental composition of the synthesized nanomaterials were examined using field-emission scanning electron microscopy (FE-SEM; JEOL JSM-6700F) and high-resolution transmission electron microscopy (HRTEM; JEOL JEM-2100F). Surface chemical states and crystallographic structures were analyzed by X-ray diffraction (MP-XRD; Malvern Panalytical / X-ray diffractometer using Cu Kα radiation), Raman spectroscopy (HORIBA, LabRAM HR Evo 800) and angle-resolved X-ray photoelectron spectroscopy (AR-XPS; Thermo Fisher Scientific K-ALPHA XPS, Al Kα radiation at 12 kV).

Electrochemical Measurement

The as-prepared nanofibers and commercial Ir/C catalyst were separately dispersed in deionized water to obtain catalyst inks with a concentration of 2 mg mL^{-1}. An aliquot (6 μL) of each well-dispersed ink was drop-cast onto a glassy carbon (GC) disk electrode (3 mm diameter) and dried in an oven at 60 °C for 10 min. This drop-casting procedure was repeated five times, resulting in a total catalyst loading of 60 μg on each electrode. Subsequently, 10 μL of 0.05 wt% Nafion solution (diluted in ethanol) was drop-cast onto the catalyst-modified GC electrode and dried in a desiccator for 30 min. All electrochemical measurements were conducted using a standard three-electrode configuration, with the catalyst-loaded GC electrode as the working electrode, a saturated calomel electrode (SCE) as the reference electrode, and a coiled Pt wire as the counter electrode. The OER activity was evaluated by rotating disk electrode (RDE) voltammetry using an electrochemical analyzer (RDE-1 rotor/Epsilon electrochemical analyzer, BASi) in N_2-saturated 1.0 M NaOH (*aq*) at a rotation rate of 1600 rpm. Current densities were calculated by normalizing the measured current to the geometric surface area (GSA) of the electrode. The GSAs were determined by chronocoulometry measurements in 0.1 M KNO_3 containing 10 mM $K_3Fe(CN)_6$ [15]. All electrochemical

measurements were performed using a CHI 920C electrochemical workstation (CH Instruments).

Acknowledgements

The authors declare that they have no known competing financial interests or personal relationships that could have appeared to influence the work reported in this paper. D.J. gratefully acknowledge support from Department of Chemistry, College of Natural Science at Jeonbuk National University.

Funding

This work was financially supported by the National Research Foundation of Korea (NRF) funded by the Ministry of Science and ICT or by the Ministry of Education (NRF-RS-2018-NR031064 and RS-2025-16063688).

References

1. Song, J.; Chitumalla, R. K; Kim, M. H.; Jang, J.; Jin. D. *Nano Energy,* **2026,** *148,* 111632.
2. Zhou, Y.; Sun, S.; Wei, C.; Sun, Y.; Xi, P.; Feng, Z.; Xu, Z.J. *Adv. Mater.*, **2019**, *31*, 1902509.
3. Zhang, K.; Ruqiang Z. *Small*, **2021**, *17*, 2100129. doi: 10.1002/smll.202100129
4. Milliken, E. C.; Cordaro, J. F. *J. Mater. Res.*, **1990**, *5* (1), 53-56.
5. Singh, J.; Kaur, G.; Rawat, M. *J. Bioelectron. Nanotechnol*, **2016**, *1* (1), 9.
6. Vernon, W. H. *J. Trans. Faraday Soc.*, **1931**, *27*, 255-277.
7. Wu, C. K.; Yin, M.; O'Brien, S.; Koberstein, J. T. *Chem. Mater.*, **2006**, *18* (25), 6054-6058.

8. Poulston, S.; Parlett, P. M.; Stone, P.; Bowker, M. *Surf. Interface Anal.*, **1996**, *24* (12), 811-820.
9. Wang, Y.; Song, Z.; Ma, D.; Luo, H.; Liang, D.; Bao, X. J. Mol. Catal. A Chem., **1999**, *149* (1-2), 51-61.
10. Ashida, T.; Miura K.; Nomoto T.; Yagi S.; Sumida H.; Kutluk G.; Soda K.; Namatame H.; Taniguchi M. *Surf. Sci.*, **2007**, *601* (18) 3898-3901.
11. Shirai, H.; Morioka, Y.; Nakagawa, I. *J. Phys. Soc. Jpn.*, **1982**, *51* (2), 592-597.
12. Yim, Y.; Park, C.; Lee, Y.; Kim, M. H. *J. Alloys Compd.*, **2025**, *1043*, 184248.
13. Ge, L.; Flynn, J.; Paddison, J. A. M.; Stone, M. B.; Calder, S.; Subramanian, M. A.; Ramirez, A. P.; Mourigal, M. *Erratum Phys. Rev. B*, **2018**, *98*, 219901.
14. Sprague, A. P.; Patterson, B. R.; Grandhi, S. *Metall. Mater. Trans. A*, **2010**, *41* (3), 592-602.
15. Sharma, J. N.; Pattadar, D. K.; Mainali, B. P.; Zamborini, F. P. *Anal. Chem.*, **2018**, *90* (15), 9308-9314.